Harmonic Radar for Differentiating Between Friend and Foe

Tanisha Gosain and Shobha Sundar Ram
Indraprastha Institute of Information Technology Delhi, New Delhi 110020 India
E-mail: {tanisha17204, shobha}@iiitd.ac.in

2021 IEEE Radar Conference (RadarConf21) | 978-1-7281-7609-3/20/$31.00 ©2021 IEEE | DOI: 10.1109/RadarConf2147009.2021.9455323

***Abstract*—We present a modified harmonic radar architecture for distinguishing between two dynamic targets - a friend and a foe - in the radar propagation channel. The main application for our proposed radar is for search and rescue missions or surveillance. The radar consists of a narrowband sinusoidal transmitter and a dual channel receiver, wherein the primary and secondary channels are tuned to the fundamental transmitted frequency and its second order harmonic respectively. The radar scattered returns from both friend and foe are gathered at the primary receiver while the secondary receiver gathers the second order harmonics emanating from the harmonic radar tag on the friend. The secondary receiver data are used to train unique data driven dictionaries that characterize the motion of the friend. These dictionaries are used to disaggregate and reconstruct the returns from the friend and foe in the primary linear radar data. We validate our proposed radar concept on simulated radar data of a friend and foe and demonstrate that the radar signatures from the reconstructed radar data are qualitatively and quantitatively similar to the ground truth radar signatures from the friend and foe.**

I. Introduction

A harmonic radar typically transmits a radar signal at a carrier frequency (f_c). This signal falls on a target that is *tagged* with a passive electronic circuit consisting of a wire dipole antenna, a Schottky diode and an inductive loop across the diode [1]. Due to the inherent non-linearity in the diode characteristics, higher order harmonics are generated in the tag of which the second order harmonic is the strongest. The returns are scattered back to the radar which consists of a radar receiver tuned to twice the carrier frequency ($2f_c$). Returns at the higher order harmonics, therefore, indicate the presence of the tagged target. Variants of the harmonic radar have been researched and developed for detecting and tracking insects (especially bees) [2]–[5]. More recently, harmonic radars have been researched for imaging moving targets and synthetic aperture imaging of targets by effectively suppressing clutter from linear targets [6], [7]. Unlike RFID tags that operate over ultra-short ranges (a few centimeters), the harmonic radar is capable of tracking cooperative targets over longer ranges (several meters).

In this work, we propose a modified architecture of a harmonic radar to distinguish between *friends* and *foes* at short ranges in the radar propagation channel. This novel variant of the harmonic radar receiver will be useful for diverse applications such as search and rescue missions in hostile environs, or for facilitating fire escape strategies, or for surveillance. For example, the radar operator will be able to track the rescue operator in the midst of hostile personnel by tagging the rescue operator with a small size, passive, harmonic radar tag. Similarly, operators outside will be able to effectively detect, monitor and guide a fireman by tagging him. In the simplest scenario, let us assume that the channel consists of two dynamic targets - a *friend* and a *foe*. In the proposed architecture, shown in Fig.1, the radar transmits a continuous wave frequency signal at f_c that falls on both friend and foe. The radar consists of two receiver channels - a primary channel (antenna, mixer, filter) tuned to f_c, like a classical linear radar, and a secondary channel tuned to $2f_c$ resembling a traditional harmonic radar receiver. The friend is distinguished from the foe by tagging the friend with a harmonic radar tag that generates second and higher order harmonics of the incoming signal. Since both the friend and foe are dynamic, they give rise to time-varying Doppler shifts that are proportional to the product of the radial velocity of their motions with respect to the radar and the carrier frequency. Hence, the scattered returns at the primary radar receiver will consist of the superposition of the Doppler shifted returns from both the friend and foe at f_c. However, the secondary receiver will gather the Doppler shifted returns from the friend alone at $2f_c$. Since the returns from the friend at both the receivers are functions of the motion of the friend, the hypothesis is that the radar data obtained from the secondary receiver can be used to disaggregate the signals from the friend and foe at the primary receiver.

Traditional data independent transforms such as Fourier and wavelets are not suitable for our problem formulation since the same set of basis vectors or dictionary atoms cannot be used for representing the signals at both f_c and $2f_c$. In [8], [9], customized basis vectors were derived from radar data at specific frequencies using sparsity based dictionary learning algorithms and used to classify data at other distinct frequencies. Since these dictionaries are fine tuned to the underlying motion characteristics of the target, the same set of dictionary atoms were effective across multiple frequencies. Using similar principles, we propose to derive customized, data driven dictionaries from the second order harmonic radar data from the friend. Then, we use these dictionary atoms in two ways on the radar data from the primary receiver. First, we reuse the friend's dictionary atoms to extract the component of the friends returns from the aggregate radar signal. Second, we use the friends dictionary to initialize the dictionary learning algorithm for the foe.

We test the algorithm on simulated radar data for the proposed modified harmonic radar architecture. We use computer animation data to model two different motions - one for the friend and one for the foe. Then we combine these animation data with electromagnetic modeling based on the techniques described in [10] to simulate the time-domain linear and harmonic radar returns at both the receivers. These modeling techniques have been widely used in radar literature to generate realistic radar micro-Doppler spectrograms of dynamic targets - humans, animals [11] and vehicles [12], [13]. We use sparsity based dictionary learning algorithms on the secondary radar receiver data to extract dictionaries for the friend. Then we reuse these same dictionaries on the radar data from the primary receiver to separate the signals from the friend and the foe.

Our paper is organized in the following manner. In the following section, we describe the proposed dictionary learning algorithm for separating the friend and foe returns from the aggregate time-domain radar data. Then in Section III, we describe the simulation methodology that we have adopted for modeling the radar returns of both the friend and the foe at the proposed harmonic radar architecture. Then in Section IV, we present the results of the algorithm on the simulated radar data. Finally, we conclude the paper in Section V. *Notation:* Upper-case bold characters are used to denote matrices, $||.||_{\mathrm{p}}$ represents the l_{p} norm of a vector.

II. Theory

In the proposed radar architecture, a continuous wave signal at carrier frequency f_c is transmitted. The radar consists of two receivers: a primary linear receiver turned to f_c, and a secondary harmonic radar receiver tuned to $2f_c$. The radar propagation channel consists of two targets - a friend and a foe. The friend is tagged with a passive electronic circuit consisting of a dipole, diode and an inductive loop. The scattered radar signal consisting of the Doppler shifted returns from the dynamic friend and foe at f_c is gathered at the primary radar receiver. The data are represented as a matrix, $\mathbf{X}^1_{\mathrm{rx}}$, with N number of measurements or time-domain signals ($\mathbf{X}^1_{\mathrm{rx}} = [x^1_{rx_1} \dots x^1_{rx_N}]$). Each of these signals is digitized to have M samples and denoted by $x^1_{rx_n} \in R^{M\times 1}$. The harmonic radar data at the secondary receiver are represented as $\mathbf{X}^2_{\mathrm{rx}}$ which has the same dimensions as $\mathbf{X}^1_{\mathrm{rx}}$. In the following two sections, we describe the algorithms for learning the friend's dictionary from $\mathbf{X}^2_{\mathrm{rx}}$ and how this dictionary can be subsequently used to separate the returns from the friend and foe in $\mathbf{X}^1_{\mathrm{rx}}$.

A. Learning Friend's Dictionary from Second Order Harmonic Radar Data

Traditionally, radar data have been expressed in terms of data independent basis vectors such as Fourier or wavelets. More recently, data driven dictionaries have been used to represent radar data [14]. The advantage here is that the atoms of the dictionaries are fine tuned to uniquely represent the radar data with greater sparsity. The resulting dictionaries have been utilized for a plethora of radar applications such as target classification [8], [9], clutter mitigation [9] and single channel source separation for detection of multiple targets [15], [16]. In this work, we use these dictionary learning algorithms to represent the radar data from the secondary receiver, as shown in

$$\mathbf{X}^2_{\mathrm{rx}} = \mathbf{D}_{\mathrm{fr}}\,\mathbf{Z}^2_{\mathrm{fr}} + \mathbf{N}_2. \tag{1}$$

Here $\mathbf{D}_{\mathrm{fr}}$ are unique and customized data driven dictionaries that represent the data with corresponding coefficients $\mathbf{Z}^2_{\mathrm{fr}}$ and $\mathbf{N}_2$ is the additive Gaussian noise in the secondary radar receiver. Our objective is to learn these dictionaries by minimizing the objective function, $J_1(\mathbf{D}_{\mathrm{fr}}, \mathbf{Z}^2_{\mathrm{fr}})$, as shown in

$$\min_{\mathbf{D}_{\mathrm{fr}},\mathbf{Z}^2_{\mathrm{fr}}} ||\,\mathbf{X}^2_{\mathrm{rx}} - \mathbf{D}_{\mathrm{fr}}\,\mathbf{Z}^2_{\mathrm{fr}}\,||^2_2 \; s.t \; ||\,\mathbf{Z}^2_{\mathrm{fr}}\,||_0 < \tau_0. \tag{2}$$

In (2), we enforce an l_0 norm ($\|.\|_0$) constraint on the coefficient matrix, $\mathbf{Z}^2_{\mathrm{fr}}$, to enforce the sparse representation of radar data. However, the l_0 minimization problem is NP-hard [17]. Therefore, using standard compressed sensing techniques, we relax the l_0-norm with l_1-norm, as shown in

$$\min_{\mathbf{D}_{\mathrm{fr}},\mathbf{Z}^2_{\mathrm{fr}}} ||\,\mathbf{X}^2_{\mathrm{rx}} - \mathbf{D}_{\mathrm{fr}}\,\mathbf{Z}^2_{\mathrm{fr}}\,||^2_2 + \lambda||\,\mathbf{Z}^2_{\mathrm{fr}}\,||_1, \tag{3}$$

and still ensure sparsity. Here $\lambda \in R$, is a regularization parameter that trades-off between the sparsity level in $\mathbf{Z}^2_{\mathrm{fr}}$ and the error in data fitting. The subsequent optimization is done through a two staged procedure where $\mathbf{D}_{\mathrm{fr}}$ and $\mathbf{Z}^2_{\mathrm{fr}}$ are updated through two alternating minimization operations as described below.

In the first step, the atoms in $\mathbf{D}_{\mathrm{fr}}$ are initialized using randomly selected training radar signals such that $\mathbf{D}_{\mathrm{fr}} \in R^{M\times P}$, is over complete ($M < P$). Then we solve for $\mathbf{Z}^2_{\mathrm{fr}}$ in

$$\min_{\mathbf{Z}^2_{\mathrm{fr}}} ||\,\mathbf{X}^2_{\mathrm{rx}} - \mathbf{D}_{\mathrm{fr}}\,\mathbf{Z}^2_{\mathrm{fr}}\,||^2_2 + \lambda||\,\mathbf{Z}^2_{\mathrm{fr}}\,||_1, \tag{4}$$

using the iterative soft thresholding algorithm (ISTA) [18]. Once the sparse coefficients are obtained, the dictionary is updated using a least squares approach [19], as shown in

$$\min_{\mathbf{D}_{\mathrm{fr}}} \left\|\mathbf{X}^2_{\mathrm{rx}} - \mathbf{D}_{\mathrm{fr}}\,\mathbf{Z}^2_{\mathrm{fr}}\right\|^2_F$$
$$s.t. \left\|d_{fr_p}\right\|^2_2 \leq 1, \forall p = 1, 2, \dots P. \tag{5}$$

Columns of the dictionary are normalized to have norm less than unity. The steps in (4) and (5) are iterated until $J_1(\mathbf{D}_{\mathrm{fr}}, \mathbf{Z}^2_{\mathrm{fr}})$ converges or reaches a very low tolerance level.

B. Disaggregation of Friend and Foe Returns from Primary Radar Data at Fundamental Frequency

The radar data at the primary receiver consists of returns from the friend and foe and hence can be written as

$$\mathbf{X}^1_{\mathrm{rx}} = \mathbf{D}_{\mathrm{fr}}\,\mathbf{Z}^1_{\mathrm{fr}} + \mathbf{D}_{\mathrm{foe}}\,\mathbf{Z}_{\mathrm{foe}} + \mathbf{N}_1, \tag{6}$$

where $\mathbf{D}_{\mathrm{foe}}$ and $\mathbf{Z}_{\mathrm{foe}}$ are the dictionaries and coefficient vectors of the foe and $\mathbf{N}_1$ is the Gaussian noise at the primary radar receiver. In the above expression, we reuse the same $\mathbf{D}_{\mathrm{fr}}$ learnt from the secondary radar receiver data to represent the

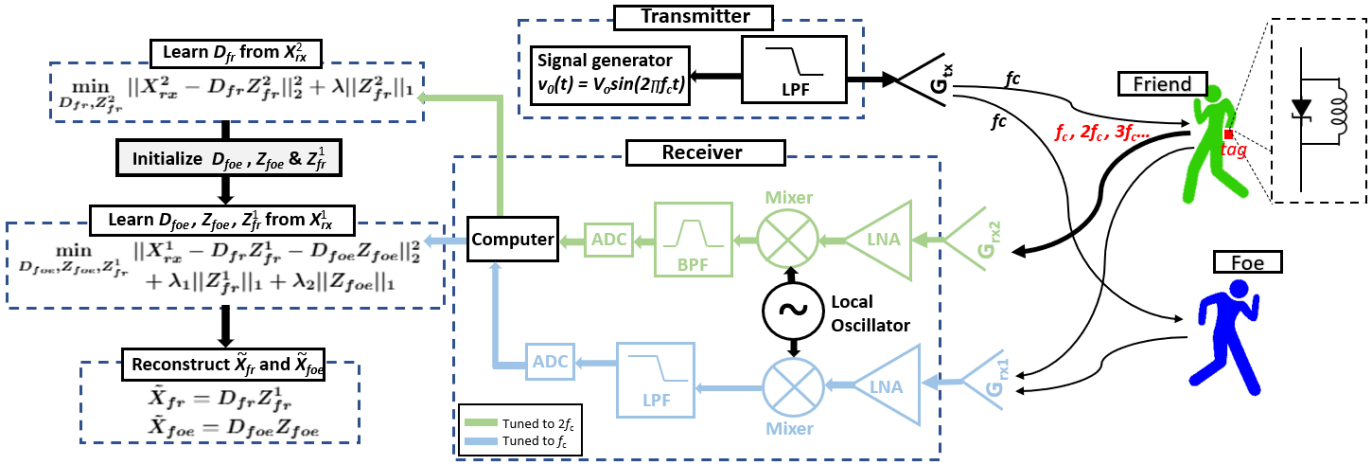

Fig. 1: System diagram of proposed harmonic radar architecture

returns from the friend. The corresponding coefficients are $\mathbf{Z}^1_{\text{fr}}$ which are naturally distinct from $\mathbf{Z}^2_{\text{fr}}$. Here, the goal is to separate the returns from the friend and foe. Hence, we formulate a second objective function, $J_2(\mathbf{D}_{\text{foe}}, \mathbf{Z}_{\text{foe}}, \mathbf{Z}^1_{\text{fr}})$, as

$$\min_{\mathbf{D}_{\text{foe}},\mathbf{Z}_{\text{foe}},\mathbf{Z}^1_{\text{fr}}} || \mathbf{X}^1_{\text{rx}} - \mathbf{D}_{\text{fr}}\,\mathbf{Z}^1_{\text{fr}} - \mathbf{D}_{\text{foe}}\,\mathbf{Z}_{\text{foe}} ||^2_2 \quad s.t\ || \mathbf{Z}^1_{\text{fr}} ||_0 < \tau_1 \text{ and } || \mathbf{Z}_{\text{foe}} ||_0 < \tau_2. \tag{7}$$

In (7), sparsity constraints have been imposed on both $\mathbf{Z}^1_{\text{fr}}$ and $\mathbf{Z}_{\text{foe}}$. Again, due to the NP-hard nature of the formulation, we use compressive sensing techniques to relax the l_0 norm to l_1 norm, as shown in

$$\min_{\mathbf{D}_{\text{foe}},\mathbf{Z}_{\text{foe}},\mathbf{Z}^1_{\text{fr}}} || \mathbf{X}^1_{\text{rx}} - \mathbf{D}_{\text{fr}}\,\mathbf{Z}^1_{\text{fr}} - \mathbf{D}_{\text{foe}}\,\mathbf{Z}_{\text{foe}} ||^2_2 + \lambda_1 || \mathbf{Z}^1_{\text{fr}} ||_1 + \lambda_2 || \mathbf{Z}_{\text{foe}} ||_1, \tag{8}$$

where λ_1 and λ_2 are the regularization parameters that control the degree of sparsity in the corresponding coefficients and the error in the data fitting.

We solve (8) through iterative steps. We begin by first initializing the values of $\mathbf{D}_{\text{foe}}$ and $\mathbf{Z}_{\text{foe}}$. $\mathbf{D}_{\text{foe}} \in R^{M\times P}$ is initialized by selecting P random signals from $\mathbf{X}^1_{\text{rx}}$ and $\mathbf{Z}_{\text{foe}} \in R^{P\times N}$ is initialized with a randomly constructed sparse matrix. Then, we estimate $\mathbf{Z}^1_{\text{fr}}$ by solving

$$\min_{\mathbf{Z}^1_{\text{fr}}} || \mathbf{X}^1_{\text{rx}} - \mathbf{D}_{\text{foe}}\,\mathbf{Z}_{\text{foe}} - \mathbf{D}_{\text{fr}}\,\mathbf{Z}^1_{\text{fr}} ||^2_2 + \lambda_1 || \mathbf{Z}^1_{\text{fr}} ||_1, \tag{9}$$

using the ISTA algorithm. Then using this estimate for $\mathbf{Z}^1_{\text{fr}}$, we solve

$$\min_{\mathbf{Z}_{\text{foe}}} || \mathbf{X}^1_{\text{rx}} - \mathbf{D}_{\text{fr}}\,\mathbf{Z}^1_{\text{fr}} - \mathbf{D}_{\text{foe}}\,\mathbf{Z}_{\text{foe}} ||^2_2 + \lambda_2 || \mathbf{Z}_{\text{foe}} ||_1, \tag{10}$$

for $\mathbf{Z}_{\text{foe}}$ again using the ISTA algorithm. Finally, we update $\mathbf{D}_{\text{foe}}$ using least squares where

$$\min_{\mathbf{D}_{\text{foe}}} || \mathbf{X}^1_{\text{rx}} - \mathbf{D}_{\text{fr}}\,\mathbf{Z}^1_{\text{fr}} - \mathbf{D}_{\text{foe}}\,\mathbf{Z}_{\text{foe}} ||^2_2 \quad s.t\ ||d_{foe_p}||^2_2 < 1, p = 1 \cdots P. \tag{11}$$

The steps in (9),(10) and (11) are repeated until the objective function converges or the data fitting error reaches a very low value.

C. Reconstructing friend and foe's returns

Once the dictionaries and the corresponding coefficients of the friend and the foe are learnt from the primary radar data, the individual returns from the friend ($\tilde{X}_{fr}$) can be reconstructed using

$$\tilde{\mathbf{X}}_{fr} = \mathbf{D}_{\text{fr}}\,\mathbf{Z}^1_{\text{fr}}\,. \tag{12}$$

Similarly the returns from the foe are reconstructed using

$$\tilde{\mathbf{X}}_{foe} = \mathbf{D}_{\text{foe}}\,\mathbf{Z}_{\text{foe}}\,. \tag{13}$$

III. Simulation Set Up

In this section, we discuss the simulation set up for validating the proposed methodology. We consider the proposed dual channel radar, transmitting a sinusoidal waveform at a carrier frequency of f_c. We assume that the radar propagation channel consists of two targets - a friend who is tagged with a harmonic radar tag and a foe. We model the radar returns from both friend and foe by combining computer animation models of human motions with radar scattering center models of the humans as described in [10], [20]. Computer animation data describe the skeleton structure of $B_i, i : fr, foe$, bones of a friend or foe and the time-varying positions of each of the joints of the skeleton. We model each of the humans as a collection of ellipsoidal primitives defined for each bone and the scattering center of each of the primitive is assumed to be located at the center of the ellipsoid. Then, the n^{th} time-domain linear radar returns at the primary receiver, $x^n_{rx_1}$, are the superposition of the returns from the friend and foe. This is modelled as

$$x^n_{rx_1}[m] = \sum_{b=1}^{B_{fr}} \frac{\sqrt{\sigma^b_{fr}[m]}}{r^b_{fr}[m]^2} e^{-j2\pi f_c 2r^b_{fr}[m]/c} + \sum_{b=1}^{B_{foe}} \frac{\sqrt{\sigma^b_{foe}[m]}}{r^b_{foe}[m]^2} e^{-j2\pi f_c 2r^b_{foe}[m]/c} \tag{14}$$

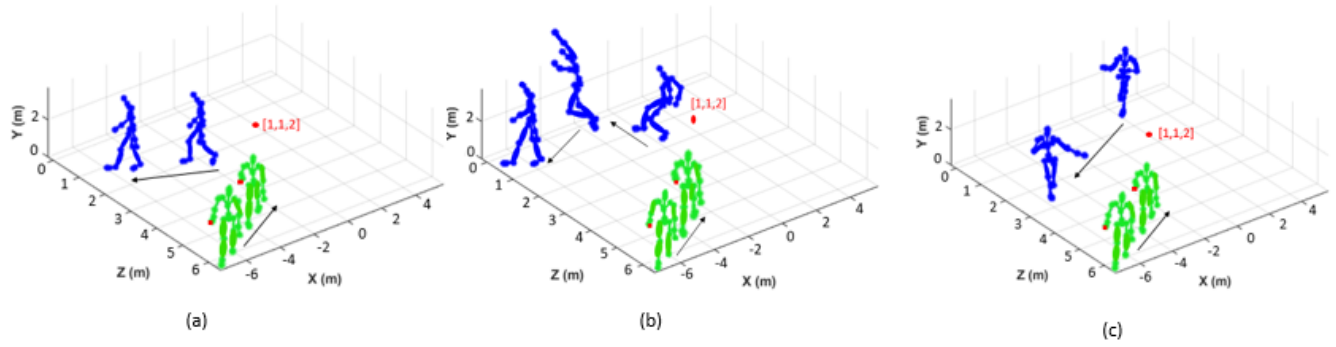

Fig. 2: Room geometry of three different scenarios where foe is (a) walking away from the radar, (b) jumping, and (c) skipping

where $\sqrt{\sigma_i^b}, i : fr, foe$, is the radar cross-section of each b^{th} ellipsoid on the friend or foe. This RCS is a function of the dimensions of the primitive, the skin dielectric properties and the radar aspect angle [21]. In (14), $r_i^b, i : fr, foe$, is the radial distance between the b^{th} point scatterer on the friend or foe from the radar. The duration of each simulation is one coherent processing interval. We consider N such simulations to form $\mathbf{X}_{\text{rx}}^1$. In a similar manner, we generate $\mathbf{X}_{\text{rx}}^2$. Here, the returns are only from the friend and not the foe since only the friend is tagged and the carrier frequency in the exponent is $2f_c$. In the above simulation model, we have assumed that there is no electromagnetic interaction (multipath scattering or shadowing) between the friend and the foe. Hence the performance of the algorithm when the friend and foe are spaced closely in range/cross-range can only be determined via experiments.

In our work, we have considered a radar of $f_c = 7.5$GHz, located at $[1, 1, 2]m$ as shown in Fig.2 where $X - Z$ plane is the ground plane and Y is the height axis. Computer animation data from ACCAD motion capture database, CMU at a video frame rate of 120 fps are used to model both the friend and the foe. The animation data are suitably interpolated from the video frame rate to the radar sampling frequency of 1KHz. The skeleton structure of the human in this data consists of 28 bones. We simulate radar returns for three different cases. For all three cases, the friend walks towards the radar from $[-6, 0, 6]m$ to $[0, 0, 0]m$ and is depicted in green in the figure. From here onwards, we refer to the friend's motion as FH. In each of the three cases, we consider a different motion for the foe - a human walking away from the radar (BH), a human running, jumping and finally walking away from the radar (RJWH) and a human skipping as it passes the radar (SH). The foe is depicted in blue in the figure. The trajectories for each of these motions are indicated in Fig.2a, b and c respectively. The dwell time / coherent processing interval for each of the simulations is $0.1s$. Hence, the entire duration of the motions are split into multiple measurements of $0.1s$ width.

IV. Results

In this section, we discuss the qualitative and quantitative results to validate our proposed methodology for distinguishing between friend and foe.

A. Qualitative Comparison

We first discuss the first case, where the friend is walking towards the radar but the foe is walking away from the radar, as shown in Fig.2a. The time domain linear radar data from the superposition of friend and foe returns, $\mathbf{X}_{\text{rx}}^1$, are processed with short time Fourier transform using a window function, $h(t)$, as shown in

$$\chi_{fr}(t, f_D) = \int x_{fr}(\tau) h(t - \tau) e^{-j2\pi f_D \tau} d\tau, \qquad (15)$$

and displayed in Fig.3. In (15), f_D indicates the Doppler frequency. Figures.3b and c show the ground truth results

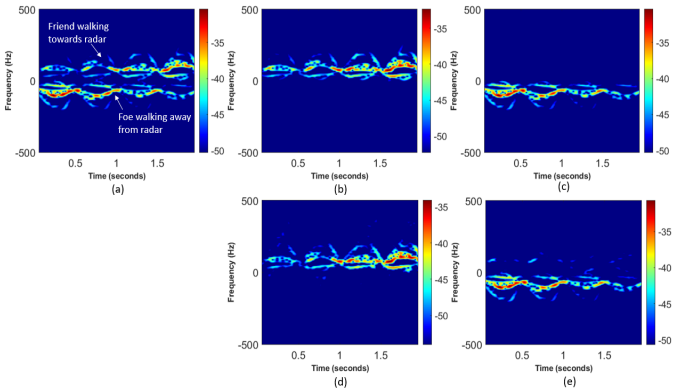

Fig. 3: Micro-Doppler spectrogram of (a) returns from friend walking toward the radar and foe walking away from radar; ground truth returns of (b) friend, and (c) foe; reconstructed returns of (d) friend, and (e) foe

for the friend (χ_{fr}) and foe (χ_{foe}) respectively. Since the friend is walking towards the radar (FH), the micro-Dopplers are positive. The strongest returns emanate from the torso while the weaker returns arise from the swinging of the arms and legs. The returns from the human walking away are very similar except that they are at negative Dopplers. The dictionaries for the friend are learned from the radar data from the second receiver and then used to extract the friend returns from the aggregate; and to learn the dictionary of the foe. The reconstructed friend ($\tilde{\chi}_{fr}$) and foe ($\tilde{\chi}_{foe}$) returns are presented in Fig.3d and Fig.3e respectively. The results for

all the figures are normalized for a dynamic range of $20dB$. Note that the spectrogram reconstructed from the dictionary learning at the second harmonic frequency captures the salient micro-Doppler features in the fundamental frequency data and closely resembles the ground truth results qualitatively. This demonstrates the efficacy of dictionary learning over traditional data independent transforms for capturing higher order motion characteristics. The strength of the returns from the reconstructed data, however, slightly differs from those of the ground truth. Thus the dictionary learning is not quite as effective in correctly estimating the signal strength. Learning the dictionary of foe data is slightly more challenging since there are no training data available (unlike the friend). The reconstructed image looks fairly similar to the ground truth data and we are able to observe the negative micro-Dopplers from the torso and the limbs. However, we observe some remnants of the friend, in the form of a few positive micro-Dopplers, in the spectrogram of the foe.

In the second case, the foe first runs, then jumps and finally resumes walking (RJWH), as shown in Fig. 2b. The micro-Doppler spectrogram generated from the superposition of the returns from the friend and foe are shown in Fig.4a and the corresponding ground truth results from each of the two humans are shown in Fig.4b and c respectively. The reconstructed results of the friend and foe are shown

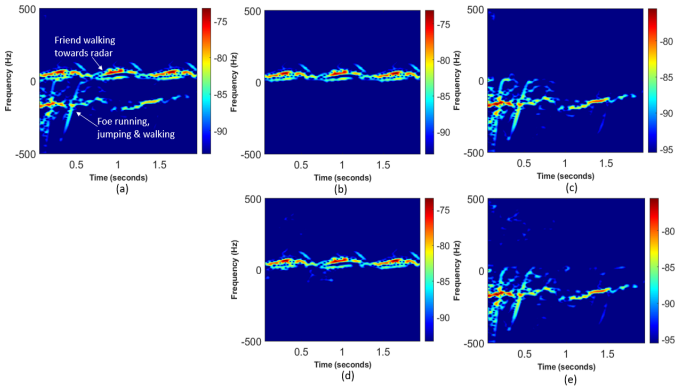

Fig. 4: Micro-Doppler spectrogram of (a) returns from friend walking toward the radar and foe running, jumping and walking; ground truth returns of (b) friend, and (c) foe; reconstructed returns of (d) friend, and (e) foe.

in Fig.4d and e respectively. Since the running motion is faster than the walking motion, we see high Dopplers at the beginning from approximately 0 to 0.5s, then we see a discontinuity arising from the jumping motion, following which the spectrogram transitions to walking motion. Again, we observe that the reconstruction of the friend from the higher order harmonic radar data is fairly effective from a qualitative perspective. However, the strength is not quite the same. The reconstructed micro-Dopplers from the foe are also fairly similar to the ground truth results. However, we again observe some additional noise-like features, at high frequencies, in the reconstructed spectrograms.

In the last case, the foe performs a skipping motion as shown in Fig.2c. The resulting spectrograms of the radar data before and after dictionary learning are presented in Fig.5. The ground truth radar micro-Dopplers show that the

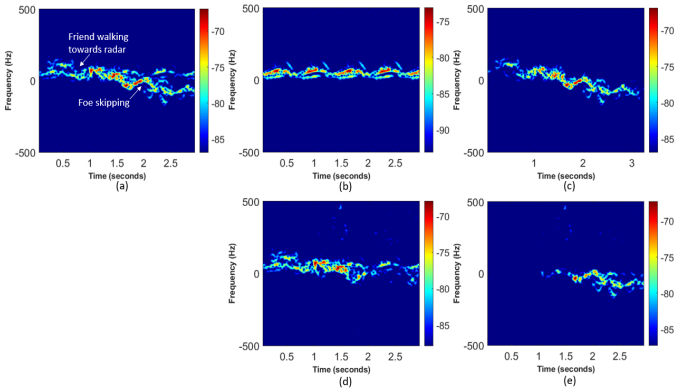

Fig. 5: Micro-Doppler spectrogram of (a) returns of friend walking toward the radar and foe skipping; ground truth returns of (b) friend, and (c) foe; reconstructed returns of (d) friend, and (e) foe.

skipping motion speed is somewhat similar to the walking motion. However, the Doppler appears to be steadily declining due to the translational trajectory adopted by the foe. In the aggregate radar data shown in Fig.5a, we observe that there is considerable overlap in the micro-Doppler between the walking and the skipping motions between 0 and 1.5s. As a result, the reconstruction of the walking motion is not as effective as the previous cases as the micro-Dopplers appear to be decreasing in Doppler. Note that the training radar data for learning dictionaries for the foe are drawn entirely from the friend data, albeit at a higher harmonic, and these dictionaries are used for reconstruction. However, the corresponding coefficients, $\mathbf{Z}^1_{\text{fr}}$, are obtained from $\mathbf{X}^1_{\text{rx}}$ which consist of returns from both friends and foes. Hence, the overlap between the friend and foe micro-Dopplers results in slightly poor estimation of $\mathbf{Z}^1_{\text{fr}}$. Similar limitations are observed in the reconstructed returns from the foe. The algorithm appears to not be able to correctly reconstruct the foe returns from 0 to 1.5s due to the overlap between friend and foe. Subsequently, it is able to correctly extract the foe. Thus the performance of the algorithm depends on the separation of the friends and foe in the micro-Doppler space.

B. Quantitative Comparison

We use two metrics of comparison between the ground truth images of the friend and foe and their corresponding reconstructed images. The first is the normalized mean square error (NMSE) that is computed by

$$NMSE = \frac{||\tilde{\chi}_{fr} - \chi_{fr}||_2^2}{||\chi_{fr}||_2^2}, \tag{16}$$

where $\tilde{X}_{fr}$ is the micro-Doppler spectrogram generated from the reconstructed time-domain returns of the friend. χ_{fr} is the micro-Doppler spectrogram obtained from the ground truth

TABLE I: Results of SSIM and NMSE: between ground-truth and reconstructed images.

Cases	Classification	SSIM	NMSE
FH (friend) + BH (foe)	Friend	0.96	0.18
	Foe	0.98	0.24
FH (friend) + RJWH (foe)	Friend	0.98	0.14
	Foe	0.97	0.17
FH (friend) + SH (foe)	Friend	0.88	0.18
	Foe	0.88	0.15

time domain data. Similar computations are conducted to determine the NMSE for the foe. NMSE is important for comparing pixel-wise the energy in both the images. However, it is not effective in comparing the gross features of both the images. Therefore, we propose a second metric called the structural similarity index (SSIM) which is computed by

$$SSIM(\tilde{\chi}_{\rm fr}, \chi_{\rm fr}) = \frac{(2\mu_{\tilde{\chi}_{\rm fr}}\mu_{\chi_{\rm fr}} + C_1)(2\sigma_{\tilde{\chi}_{\rm fr}\,\chi_{\rm fr}} + C_2)}{(\mu^2_{\tilde{\chi}_{\rm fr}} + \mu^2_{\chi_{\rm fr}} + C_1)(\sigma^2_{\tilde{\chi}_{\rm fr}} + \sigma^2_{\chi_{\rm fr}} + C_2)} \tag{17}$$

This metric compares the luminance and contrast in the two images. Here $\mu_{\chi_{\rm fr}}$, $\mu_{\tilde{\chi}_{\rm fr}}$, $\sigma_{\chi_{\rm fr}}$, $\sigma_{\tilde{\chi}_{\rm fr}}$ and $\sigma_{\tilde{\chi}_{\rm fr}\,\chi_{\rm fr}}$ are the local means, standard deviations and the co-variance of $\chi_{\rm fr}$ and $\tilde{\chi}_{\rm fr}$ respectively. The NMSE and SSIM for all three cases for both the friend and foe are reported in Table.I. The results show that the SSIM between the original ground truth images and their reconstructed counterparts is fairly high for all three cases. This agrees with our qualitative observations of the similarity in the micro-Doppler features in the original images and the reconstructed images. However, the NMSE in all cases is high due to the poor estimation of the strength of the returns. Again, this result is consistent with our qualitative observation of the difference in strength.

V. Conclusion

We have proposed a harmonic radar with a dual channel receiver for distinguishing a friend and foe that are moving together in the radar propagation channel. The proposed radar framework may be useful in search and rescue missions and surveillance operations. The radar consists of a primary and secondary receiver channel that are tuned to the fundamental and second order harmonic of the transmitted signal frequency respectively. The friend, being tagged with a harmonic radar tag, scatters radar signals that are gathered by both the receivers. However, radar returns from the foe who is not tagged will only be gathered at the primary receiver. We have proposed an algorithm where the friend's radar data at the secondary receiver are used to train data driven, sparsity based dictionaries. These are subsequently used to extract the friend's radar data from the aggregate data in the primary receiver and to reconstruct the foe. We tested the proposed algorithm with simulated radar data of diverse motions of the friend and foe. Then we, qualitatively and quantitatively, compared the reconstructed radar data with the ground truth radar data. Our results showed that the proposed dictionary learning based algorithm is effective in reconstructing the salient micro-Doppler features in the friend and foe resulting in high structural similarity index values. However, there are two limitations. The algorithm is not able to correctly estimate the strength of the returns from the friend and foe resulting in poor NMSE. Second, the algorithm's performance deteriorates when there is considerable micro-Doppler overlap between the friend and foe.

References

[1] M. E. O' Neil, D. Landis, E. Rothwell, L. Kempel, and D. Reinhard, "Tracking insects with harmonic radar: a case study," *American Entomologist*, vol. 50, no. 4, pp. 212–218, 2004.

[2] B. G. Colpitts and G. Boiteau, "Harmonic radar transceiver design: miniature tags for insect tracking," *IEEE Transactions on Antennas and Propagation*, vol. 52, no. 11, pp. 2825–2832, 2004.

[3] S. Wolf, D. P. McMahon, K. S. Lim, C. D. Pull, S. J. Clark, R. J. Paxton, and J. L. Osborne, "So near and yet so far: harmonic radar reveals reduced homing ability of nosema infected honeybees," *Plos one*, vol. 9, no. 8, p. e103989, 2014.

[4] D. Milanesio, M. Saccani, R. Maggiora, D. Laurino, and M. Porporato, "Recent upgrades of the harmonic radar for the tracking of the asian yellow-legged hornet," *Ecology and evolution*, vol. 7, no. 13, pp. 4599–4606, 2017.

[5] F. Mumtaz, S. S. Ram, and S. R. Purandare, "S/c band harmonic radar for honey bee detection," in *2019 IEEE MTT-S International Microwave and RF Conference (IMARC)*. IEEE, 2019, pp. 1–5.

[6] K. A. Gallagher, G. J. Mazzaro, A. F. Martone, K. D. Sherbondy, and R. M. Narayanan, "Derivation and validation of the nonlinear radar range equation," in *Radar Sensor Technology XX*, vol. 9829. International Society for Optics and Photonics, 2016, p. 98290P.

[7] K. Gallagher, R. Narayanan, G. Mazzaro, A. Martone, and K. Sherbondy, "Static and moving target imaging using harmonic radar," *Electronics*, vol. 6, no. 2, p. 30, 2017.

[8] S. Vishwakarma and S. S. Ram, "Dictionary learning for classification of indoor micro-doppler signatures across multiple carriers," in *2017 IEEE Radar Conference (RadarConf)*. IEEE, 2017, pp. 0992–0997.

[9] ——, "Dictionary learning with low computational complexity for classification of human micro-dopplers across multiple carrier frequencies," *IEEE Access*, vol. 6, pp. 29 793–29 805, 2018.

[10] S. S. Ram and H. Ling, "Simulation of human microdopplers using computer animation data," in *2008 IEEE Radar Conference*. IEEE, 2008, pp. 1–6.

[11] ——, "Microdoppler signature simulation of computer animated human and animal motions," in *2008 IEEE Antennas and Propagation Society International Symposium*. IEEE, 2008, pp. 1–4.

[12] G. Duggal, K. V. Mishra, and S. S. Ram, "Micro-doppler and micro-range detection via doppler-resilient 802.11ad-based vehicle-to-pedestrian radar," in *IEEE Radar Conference 2019*, 2019, pp. 1–6.

[13] G. Duggal, S. Vishwakarma, K. V. Mishra, and S. S. Ram, "Doppler-resilient 802.11ad-based ultra-short range automotive joint radar-communications system," *IEEE Transactions on Aerospace and Electronic Systems*, 2020.

[14] G. Li and S. S. Ram, "Sparsity-driven methods for micro-doppler detection and classification," *Micro-Doppler Radar and its Applications*, p. 75, 2020.

[15] S. Vishwakarma and S. S. Ram, "Classification of multiple targets based on disaggregation of micro-doppler signatures," in *2016 Asia-Pacific Microwave Conference (APMC)*. IEEE, 2016, pp. 1–4.

[16] ——, "Detection of multiple movers based on single channel source separation of their micro-dopplers," *IEEE Transactions on Aerospace and Electronic Systems*, vol. 54, no. 1, pp. 159–169, 2017.

[17] B. K. Natarajan, "Sparse approximate solutions to linear systems," *SIAM journal on computing*, vol. 24, no. 2, pp. 227–234, 1995.

[18] I. W. Selesnick, "Sparse signal restoration," *Connexions*, pp. 1–13, 2009.

[19] C. M. Bishop, "Pattern recognition," *Machine Learning*, vol. 128, pp. 1–58, 2006.

[20] S. S. Ram, C. Christianson, Y. Kim, and H. Ling, "Simulation and analysis of human micro-dopplers in through-wall environments," *IEEE Transactions on Geoscience and remote sensing*, vol. 48, no. 4, pp. 2015–2023, 2010.

[21] G. Ruck, *Radar Cross Section Handbook: Volume 1*. Springer, 1970, vol. 1.